



A novel nanocomposite of polyaniline and $\text{Fe}_{0.01}\text{Ni}_{0.01}\text{Zn}_{0.98}\text{O}$: Photocatalytic, electrical and antibacterial properties



Shashi Kant^a, Susheel Kalia^b, Amit Kumar^{a,*}

^a Department of Chemistry, Himachal Pradesh University, Summer Hill, Shimla 171 005, India

^b Department of Civil, Chemical, Environmental and Materials Engineering, University of Bologna, Via Terracini 28, 40131 Bologna, Italy

ARTICLE INFO

Article history:

Received 12 April 2013

Received in revised form 12 May 2013

Accepted 16 May 2013

Available online 25 May 2013

Keywords:

Nanocomposite

Conducting polymer

Conductivity

Photodegradation

HRTEM

Antibacterial properties

ABSTRACT

A novel composite of $\text{Fe}_{0.01}\text{Ni}_{0.01}\text{Zn}_{0.98}\text{O}$ nanoparticles (FNZPs) and conducting polymer polyaniline (PANI) was synthesized by in situ free radical polymerisation method. Iron/nickel co-doped zinc oxide nanoparticles (NPs) were synthesized by sol–gel technique. The NPs and $\text{Fe}_{0.01}\text{Ni}_{0.01}\text{Zn}_{0.98}\text{O}$ /polyaniline nanocomposites (FNZP/PANI) were characterized by FTIR, EDX, SEM, HRTEM, SAED, UV–Vis and XRD techniques. Optical and photocatalytic studies revealed that formation of composite further lowers the optical band gap of FNZPs, leading to enhanced visible light absorption. Admirable photodegradation efficiency against methylene blue dye (MB) was achieved for composites. The electrical conductivity was also enhanced. The antibacterial activity of the synthesized NPs and nanocomposites (NCs) against *Escherichia coli* (*E. coli*) bacteria was analyzed by optical density method.

© 2013 Elsevier B.V. All rights reserved.

1. Introduction

In the recent years, the synthesis and engineering of inorganic/organic hybrid materials in nano-scale have received great attention due to wide range of applications. Organic–inorganic composites may combine the advantages of both components and may offer special properties through reinforcing or modifying each other. Polymer matrices reinforced with inorganic nanoparticles combine the functionalities of polymer such as low weight and ease of synthesis with unique features of inorganic nanoparticles [1]. Research is also evolving towards materials that are designed to perform more complex and efficient tasks. Examples include materials that bring about a higher rate of decomposition of pollutants, a selective and sensitive response toward a given bio-molecule, an improved conversion of light into current or more efficient energy storage. For such and more complex tasks to be realized, novel materials have to be based on several components whose spatial organization is engineered at the molecular level. Zinc oxide is a popular semiconductor oxide with wide tunable band gap (3.37 eV) and large exciton binding energy (60 MeV) [2]. The incorporation of nano-fillers into polymer matrix provides opportunities to enhance the properties of conventional composite materials [3]. The conducting polyaniline (PANI) is one of the best known conducting polymers due to its high conductivity, ease of preparation,

good environmental stability and large variety of applications [4] which make it suitable for gas sensor, as pH switching electrical conducting biopolymer hybrid for sensor applications [5], as an electrically active redox biomaterial, as a matrix for preparation of conducting polymer NCs [6,7]. Therefore, there has been a revolutionary progress in the preparation of nanocomposites based on PANI. Polyaniline is the only conducting polymer whose electrical properties can be controlled suitably by charge-transfer doping and/or protonation. Inorganic–organic composite materials are important due to their extraordinary properties, which arise from the synergism among the properties of the components. These materials are seeking much interest due to the remarkable change in properties such as mechanical [8], thermal [9–11], electrical [12], and magnetic [13] compared to pure organic polymers. Toxic effluents from industries are a matter of serious concern for the environment. Wide metal oxide semiconductors are attractive candidates for the removal of pollutants in water as they are capable of acting as catalysts upon exposure to light radiation to degrade harmful contaminants as dyes. The hybrid organic–inorganic nanomaterials can prove to be better agents.

Our synthesized FNZP/PANI hybrid nanocomposite is one of its kinds which combine the benefits of dopants (transition metal ions) and conducting polymer along with semiconductor metal oxide (ZnO). The Polyaniline acts as sensitizer thus enhances the light absorption. We have utilized this product for removal of notorious dye as methylene blue (MB) from aqueous medium. The nanocomposite has exceptionally good antibacterial activity against *E. coli*.

* Corresponding author. Tel.: +91 177 2830944.

E-mail addresses: mittuchem83@gmail.com, drsklomes@rediffmail.com (A. Kumar).

2. Materials and methods

2.1. Synthesis

All the chemicals used in synthesis were of analytical grade. Zinc nitrate, aniline, ferric nitrate and nickel nitrate and citric acid were procured from MERCK India and used as received.

For the synthesis of $\text{Fe}_{0.01}\text{Ni}_{0.01}\text{Zn}_{0.98}\text{O}$ nanoparticles Zn (NO_3)₂ (11.652 g), Ni (NO_3)₂ (0.162 g) and $\text{Fe}_2(\text{NO}_3)_3$ (0.073 g) were mixed and dissolved in 100 ml double distilled water. Citric acid (4.66 g) was added to this suspension with constant stirring. The pH of reaction mixture was kept 7 by adding liquid NH_3 solution drop wise. The solution was then dried at 80 °C to obtain a gel. The gel was then grinded and sintered at 600 °C for 2 h.

The FNZP/PANI nanocomposite was prepared by in situ free radical polymerisation of aniline. 500 mg of FNZP nanoparticles was dispersed in 100 ml of water and 50 ml of 10% aniline solution (in 1 M HCl) and 50 ml of 0.1 M Ammonium persulphate (in 1 M HCl) were added drop wise to this. The mixture was allowed to stir in ice bath (0–5 °C) for 3 h and then kept overnight for digestion. The sample was then centrifuged to remove soluble impurities and side products.

2.2. Characterization

The Phase purity and crystalline size of FZNPs and FNZP/PANI were determined by an XPERT-PRO X-ray diffractometer using Cu K α radiation. Morphological properties of NPs and NCs were studied using a Scanning Electron Microscope (SEM) QUANTA250 FEI D9393. Elemental analysis was done by EDX equipped with SEM. TEM analysis was done by High Resolution Transmission Electron Microscopy (HRTEM) and Small Area Electron Diffraction (SAED) using FEI Tecnai F20 Transmission Electron microscope. FTIR spectra were recorded with a Nicolet 5700 FTIR spectrophotometer by KBr pellet method.

2.3. Optical and photocatalytic studies

The optical band gap was studied using UV spectrophotometer. 2 mg of sample was dispersed and ultrasonicated in ethanol. UV-visible spectra were obtained using double beam spectrophotometer. The photocatalytic efficiency of the samples was studied for degradation of methylene blue as a pollutant in presence of natural sunlight in a slurry type batch reactor. The slurry consisting of MB dye and catalyst suspension was stirred magnetically. 0.25 mg/ml of photocatalyst (FNZP/PANI) was added to aqueous solution of dye (1.5×10^{-5} M). Before exposing the solutions to sunlight, they were kept in dark for 1 h to establish adsorption-desorption equilibrium. After intervals of time, aliquot of 3 ml was taken out and centrifuged to remove catalyst from suspension. The absorbance of MB solution was then recorded using double beam spectrophotometer at 662 nm. The average intensity of sunlight was recorded as $34 \times 10^3 \pm 100$ lx using Lux-meter. All experiments were performed three times and average values were reported. The effect of initial MB concentration on the degradation rate was also studied. For this 80 μM , 140 μM , 160 μM concentrations of MB were prepared. This is done to prove that dye removal is not an adsorption controlled process (Langmuir–Hinselwood mechanism).

2.4. Electrical studies

For electrical conductivity measurements, powdered samples of NPs were pressed uniaxially into pellets of 1–2 mm thickness and 8 mm diameter by applying pressure of 4 ton for 5 min. The pellets were sintered at 300 °C for NPs to get the thermal stability. Fine quality silver paint was applied on both sides of the pellets for good electrical contacts. DC electrical conductivity measurement was done using Keithley 2611 SYSTEM source meter (electrometer) by two probe method. For studying the dc conductivity of FNZP/PANI, pellet was formed without the binder by applying high pressure of 6 ton for 5 min (sintered at 100 °C). The electrical conductivity was then obtained using electrometer by four probe method.

2.5. Antimicrobial activity

The strains of *E. coli* (MTCC 739) were obtained from IMTech Chandigarh, India. The Muller Hinton Broth (Analytical Grade) was procured from Hi Media, India. Antibacterial activity of synthesized materials against *E. coli* was determined based on batch cultures containing different concentrations of FNZPs in suspension (80, 100, 140, and 160 $\mu\text{g}/\text{mL}$ prepared in dimethyl sulphoxide). After adding the samples, sterile conical flasks containing 200 mL Nutrient Broth medium were sonicated for 10 min to prevent aggregation of the NPs. The flasks were then inoculated with 1 mL of the freshly prepared bacterial suspension (Colony forming units 10^8) as per McFarlands standards [14]. The flasks were then incubated in an incubator shaker at 200 rpm and 37 °C. Bacterial growth was measured by growth curve method by measuring the increase in Optical Density (O.D) at 600 nm using a UV spectrophotometer. A positive control (containing NPs and nutrient medium, without inoculum) was also kept. The concentrations of FNZP/PANI used for testing antibacterial susceptibility were 40, 60, 80 and 100 $\mu\text{g}/\text{mL}$.

3. Results and discussions

3.1. Characterization

3.1.1. XRD analysis

The XRD pattern of the FNZPs (Fig. 1a) reveals that there is no change in the wurtzite structure of ZnO after Ni/Fe doping. The XRD pattern for FNZP show broad peaks at the positions of 31.5661, 34.4417, 36.2883, 47.6271, 56.6760, 62.7747, 66.2951, 67.7269, 69.1416 and 72.5094, which are in good agreement with the standard JCPDS file No. 30-1451 for ZnO and can be indexed as the hexagonal wurtzite structure of ZnO having space group P63mc. The average grain size of the particle has been evaluated from FWHM that is full width at the half maximum of the reflection of maximum intensity in the XRD pattern using Scherrer's formula. The average crystallite size for NPs is 31 nm and for NC is 53 nm. The d spacing is calculated using Bragg's diffraction law

$$n\lambda = 2d \sin \theta \quad (1)$$

The calculated d spacings for various planes are reported in Table 1. The crystallite size was determined using Scherrer's formula

$$p = \frac{k\lambda}{\beta \cos \theta} \quad (2)$$

where p is the crystallite size, β is the full width at half maximum, $K = 0.9$ and $\lambda = 1.54$ Å for Cu K α radiation

The lattice constants for FNZPs as calculated from XRD data were $a = b = 3.2492$ Å and $c = 5.2357$ Å. XRD diffraction pattern of FNZP/PANI (Fig. 1b) shows peak at about $2\theta = 25.82^\circ$, which is a characteristic peak of PANI [15,16] which corresponds to (110) plane of PANI [16] representing scattering from PANI chains at inter planar spacing. The peak at $2\theta = 19^\circ$ corresponds to (200) plane of PANI. In case FNZP/PANI, peaks corresponding to diffraction from (100), (002) and (103) planes of ZnO are retained. The other peaks are not visible which may be due to low FNZP and PANI molar ratio. The d spacing for (100) plane of PANI in XRD pattern of composite is 4.624 Å and for (200) plane is 3.438 Å. The composite on a whole has a semi-crystalline structure.

3.1.2. FTIR analysis

The FTIR spectrum of Ni/Fe doped ZnO (Fig. 2a) has a strong absorption band at 498.0 cm^{-1} which is Zn–O stretching frequency [17]. The peaks at 3401.3 cm^{-1} and 1561.9 cm^{-1} represents O–H and C=O stretching modes respectively. Characteristic

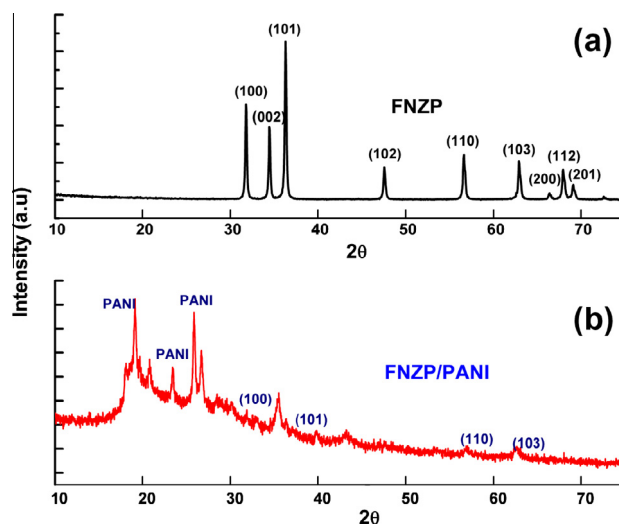


Fig. 1. XRD pattern of (a) FNZPs and (b) FNZP/PANI.

absorption peaks of PANI (Emeraldine form) and ZnO obtained from FTIR spectrum of FNZP/PANI (Fig. 2c) are 658 cm^{-1} for C–C bonding mode of aromatic ring, 848 cm^{-1} for C–H out of plane bonding in benzenoid ring, 1241 cm^{-1} for C–N stretching of benzenoid ring, 1375 cm^{-1} for C–N stretching in the neighborhood of quinoid ring [17], 3054 cm^{-1} for Symmetric stretch vibration band of methylene $[-(\text{CH}_2)_n-]$ and methyl $-(\text{CH}_3)$, 3266 cm^{-1} for interaction between ZnO and PANI by formation of hydrogen bonding between H–N and oxygen of ZnO, 486 cm^{-1} for Zn–O bond stretching and 504 cm^{-1} for Fe–O bond stretching. The characteristic peaks of PANI (Fig. 2b) at 1585 cm^{-1} , 1375 cm^{-1} , 1177 cm^{-1} , 1511 cm^{-1} are shifted to 1582 cm^{-1} , 1375 cm^{-1} , 1135 cm^{-1} , 1508 cm^{-1} respectively. This shift in peaks of PANI may be due to interaction between PANI chains and FNZP nanoparticles which results in change in electron density and bond energies of PANI. [18,19]

3.1.3. SEM/EDX analysis

Fig. 3a and b illustrates the SEM images of FNZP and FNZP/PANI respectively. The SEM micrograph shows that FNZP nanoparticles are spherical in shape with a little agglomeration. There is also some porosity which may be due to sintering process. The SEM micrograph of FNZP/PANI shows a hierarchical morphology as compared to nanoparticles and has leafy flakes like structure. The elemental analysis (EDX) of FNZP and FNZP/PANI is shown in Fig. 3e and f respectively. The percentage composition of doped samples is nearly close to the starting composition. The EDX report of the prepared NC shows the successful incorporation of PANI on to the FNZPs. The Figure shows the presence of C, N, Fe, Ni Zn and O in the nanocomposite.

3.1.4. TEM analysis

The HRTEM pictures of FNZPs (Fig. 4a) show that the particles have mixed shapes. The TEM micrographs reveal a wide distribution of hexagonal and spherical particles. The fringes in individual NPs are clearly visible and SAED pattern (Fig. 4b) reveals the perfect crystalline structure. The TEM micrograph of FNZP/PANI composite (Fig. 4c) shows that NPs are homogeneously dispersed in the PANI matrix. Fig. 4d illustrates SAED pattern of FNZP/PANI. It shows that the composite has a semi-crystalline structure. The average particle size of FNZPs is 15–30 nm and of composite is 30–50 nm.

3.2. Optical and photocatalytic studies

The UV–Visible absorption spectrum of the FNZPs (Fig. 5a) represents a sharp absorption peak around 385 nm which is the characteristic single peak of hexagonal ZnO NPs. But there is a shift in the absorption towards the longer wavelength because of doping

by transition metal ions (bare ZnO absorb at 378 nm). However, intensity of this peak decreases in case of UV–Vis spectrum of composite (Fig. 5a). A higher visible absorption can be observed in case of FNZP/PANI. The band gaps of nanoparticles and composite were calculated using Tauc relation [20]

$$\alpha hv = B(hv - E_g)^n \quad (3)$$

where α = Absorption coefficient = $2.303 A/l$, E_g = optical band gap, B = Band tailing parameter, hv is the photon energy, and $n = 1/2$ for direct band gap. The optical band gap is determined by extrapolating the straight portion of curve between $(\alpha hv)^2$ and hv when $\alpha = 0$.

The band gap as calculated from Tauc plots (Fig. 5c) for FNZPs is 3.17 eV and for FNZP/PANI (Fig. 5d) is 2.70 eV.

The photocatalytic degradation of MB in presence of FNZP and FNZP/PANI as catalysts was investigated under sunlight irradiation. The change in absorption spectra of MB in presence of photocatalysts FNZP and FNZP/PANI are shown in Fig. 5c and d respectively. Electron–hole pairs are generated during irradiation of FNZPs with UV–Visible light, which further react with water to produce hydroxyl and super-oxide radicals which disrupt the conjugation in organic molecules such as dye. This mechanism is represented in Fig. 6. Electrons and holes generated on absorption of sunlight interact with water and oxygen to form $\text{OH}\cdot$ which disrupts the conjugation in organic dye and may also mineralize it. The mechanism also shows that PANI acts as sensitizer.

The band gap of ZnO is 3.37 eV, which can be overcome by absorbing UV and visible light. But photocatalytic activity is less in sunlight (contains only 3–5% UV). The absorption is increased on doping. The effect of transition metal ions dopants on the photocatalytic activity is the dynamics of electron–hole recombination and interfacial charge transfer. The dopant ions can function as both hole and electron traps or they can mediate interfacial charge transfer. The photocatalytic efficiency can be further enhanced by incorporating the doped ZnO nanoparticles into polymer matrix as polyaniline.

As visible from absorption spectra of dye the degradation in case of FNZP/PANI is higher, it can be inferred that PANI accelerates the photodegradation process. When the NC is illuminated under natural sunlight, both FNZPs and PANI absorb the photons. The conduction band of ZnO and the Lowest Unoccupied Molecular Orbital (LUMO) of the PANI are equivalent in energy [21]. The electrons from LUMO of PANI are transferred to valence band giving rise to a new band below conduction band, thus decreasing the band gap and also enhance the photocatalytic activity. Conductive polymers as PANI act as good hole conducting material. These conductive polymers act as a stabilizer or surface capping agents when combined with metals or semiconductor nanoparticles. The disappearance of characteristic absorption peak at 662 nm after 5 h shows that dye has degraded. The % Degradation of dye is calculated as

$$\% \text{Degradation} = \frac{C_0 - C_t}{C_0} \times 100 \quad (4)$$

where C_0 is the initial concentration of dye before illumination and C_t after time t . The extent of degradation of MB (Fig. 7a) after 5 h of irradiation in presence of FNZP/PANI was 99.47% while 79% degradation is achieved in case of FNZP. The FNZP/PANI nanocomposite degrades dye to 98.55% in just 2 h after which degradation rate is almost constant and after 5 h of illumination the degradation percentage is 99.47%. Several reports claim that the rate of photodegradation of various dyes fitted a pseudo first order kinetic model [22].

Table 1

d spacings for various planes for FNZPs and FNZP/PANI.

S. no.	Diffraction plane for $\text{Fe}_{0.01}\text{Ni}_{0.01}\text{Zn}_{0.98}\text{O}$	<i>d</i> spacing (Å)
1.	100	2.813
2.	002	2.601
3.	101	2.475
4.	102	1.909
5.	110	1.622
6.	103	1.476
7.	200	1.404
8.	112	1.377
9.	201	1.371
Peaks for PANI	$\text{Fe}_{0.01}\text{Ni}_{0.01}\text{Zn}_{0.98}\text{O/PANI}$ (plane)	<i>d</i> spacing (Å)
$2\theta = 19.31^\circ$	100	4.624
$2\theta = 25.72^\circ$	200	3.438

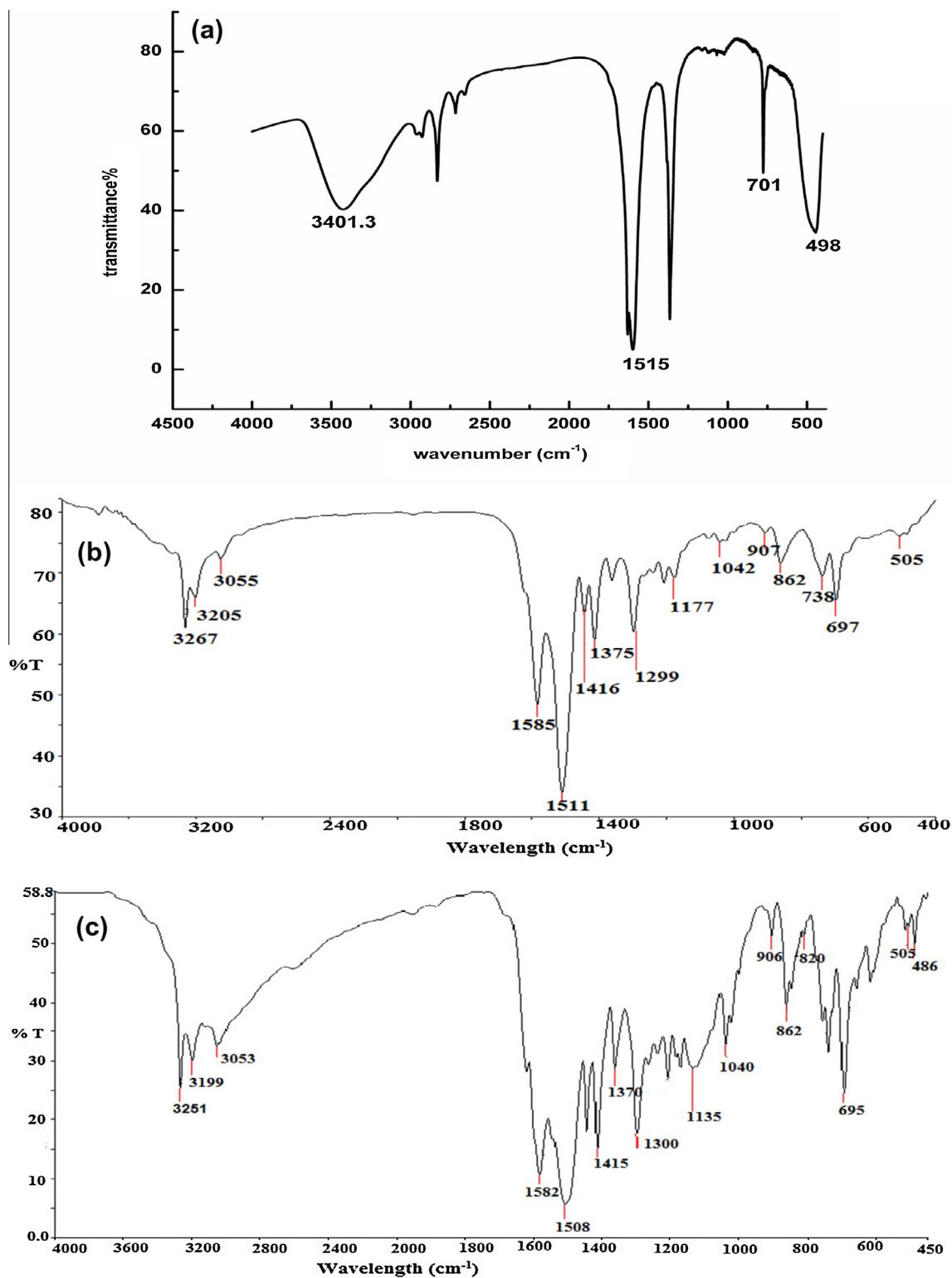


Fig. 2. (a) FTIR spectrum of FNZPs, (b) FTIR spectrum of PANI and (c) FTIR spectrum of FNZP/PANI.

$$\ln(C_0/C_t) = k_{app} t \quad (5)$$

where k_{app} is the apparent rate constant, C_0 is the concentrations of dye before illumination and C_t is the concentration of dyes at time t . Fig. 7c and d shows that the linear correlation of the plots of $\ln(C_0/C_t)$ versus time for FNZP and FNZP/PANI suggesting a pseudo first-order reaction. The value of k_{app} for

FNZPs is 0.02037 min^{-1} and for FNZP/PANI is 0.02887 min^{-1} which clearly indicates the degradation rate is faster in case of FNZP/PANI.

To confirm that the degradation of MB in our experiment is due to the photocatalytic process and is not any adsorption controlled process, the Langmuir–Hinshelwood was used for verification [23,24]:

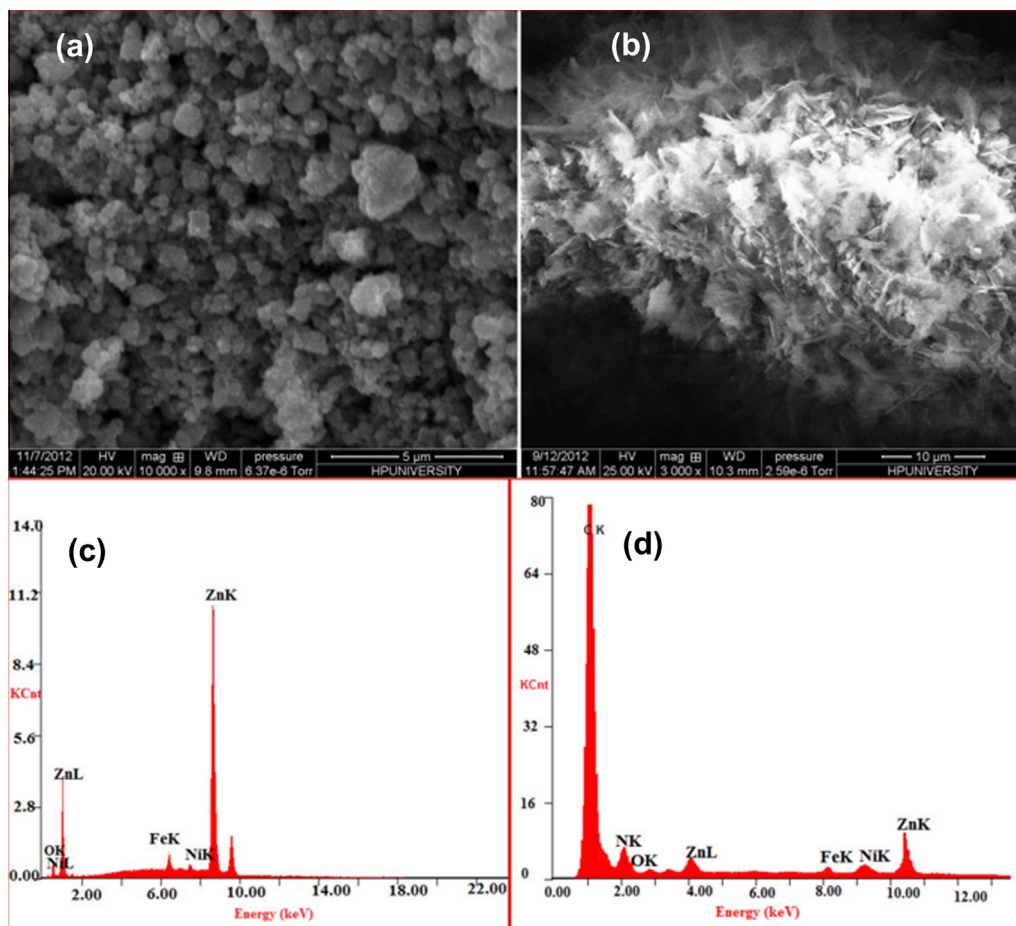


Fig. 3. (a) SEM micrograph of FNZP, (b) SEM micrograph of FNZP/PANI, (c) EDX pattern of FNZP/PANI and (d) EDX pattern of FNZPs.

$$\frac{1}{k_{app}} = \frac{1}{kK} + \frac{C_0}{k} \quad (6)$$

Table 2 shows the variation of apparent rate constant with initial MB concentration. Fig. 7d illustrates the plot of $1/k_{app}$ against C_0 at various C_0 . A linear relationship between $1/k_{app}$ and initial MB concentrations confirms the photocatalytic degradation of MB by the FNZPs and FNZP/PANI follow the Langmuir–Hinshelwood model. The degradation process is purely a photocatalysis reaction.

3.3. Electrical studies

The DC conductivity is measured using Keithley source meter. The characteristic I – V (current–voltage) curve is obtained. Using values of I and V the DC conductivity will be calculated by formula

$$\sigma = \frac{It}{VA} \quad (7)$$

The DC electrical conductivity of FNZPs and FNZP/PANI at various temperatures is shown in Fig. 8a and b respectively. This electrical conductivity depends on the intrinsic defects generated during synthesis and by the presence of dopants. The oxygen vacancies created during combustion process are responsible for electrical conductivity. The increase of electrical conductivity with temperature shows the semiconducting behavior of FNZPs [25]. It was observed that at room temperature, d c conductivity

of nanocomposite is $1.65 \times 10^{-2} \text{ S/cm}$ which is far larger than of FNZP ($2.29 \times 10^{-8} \text{ S/cm}$), though it is lower than of pure PANI. This may be due to the partial blockage of conductive paths by FNZPs embedded in PANI matrix for charge carriers which do not have sufficient energy to hop between favorite sites [26]. The decrease in the conductivity of the nanocomposites as compared to PANI was attributed to the increased charge carrier scattering between doped PANI and FNZP. As FNZP nanoparticles embedded in the PANI matrix interrupted the doping process, interactions between FNZPs and PANI increased the localization of charge carriers, and thus decreased the conductivity of the composites. However DC conductivity of FNZP/PANI is manifold as compared to FNZP.

3.4. Antibacterial studies

The growth curve studies of *E. coli* in presence synthesized NPs and NCs showed that these are effective in destruction of bacteria. It was observed that a level of $80 \mu\text{g/ml}$ of FNZPs totally inhibited the growth of general strain of *E. coli* throughout the 24 h period of incubation (Fig. 8c). However FNZP/PANI at $40 \mu\text{g/ml}$ inhibited the growth completely (Fig. 8d). However the inhibition was very slow for first 6 h. Composite well inhibited the growth for 24 h at the concentration of $60 \mu\text{g/ml}$. As observed $60 \mu\text{g/ml}$ FNZP/PANI did results in high turbidity but there was no apparent change over time, thus showed bacterial inhibition. The death phase of the *E. coli* was observed after 18 h of incubation. In tests, FNZP/PANI exhibited better bacterial inhi-

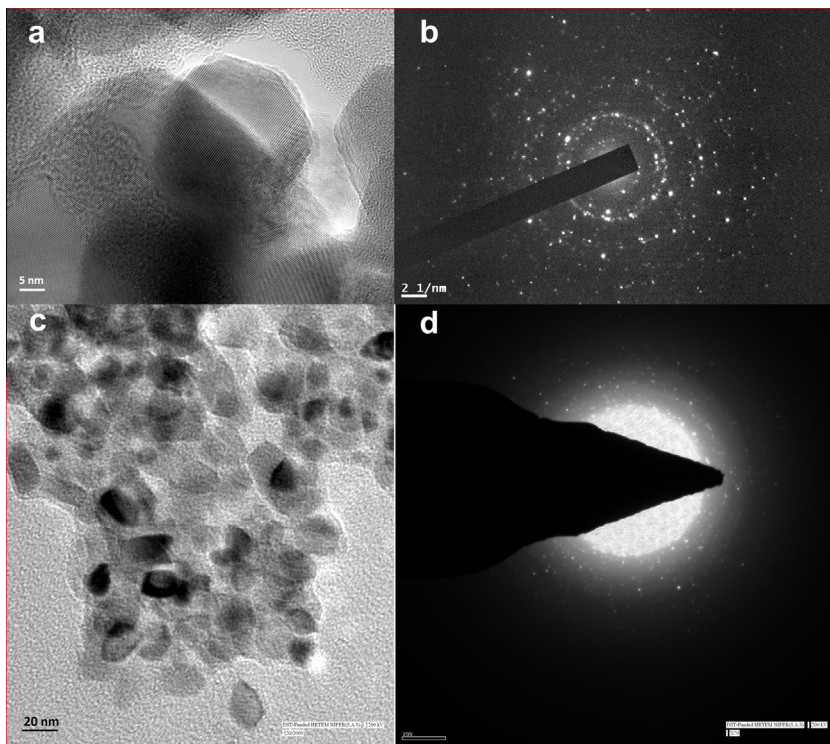


Fig. 4. (a) HRTEM image of FNZP (b) SAED pattern of FNZP (c) TEM micrograph of FNZP/PANI and (d) SAED pattern of FNZP/PANI.

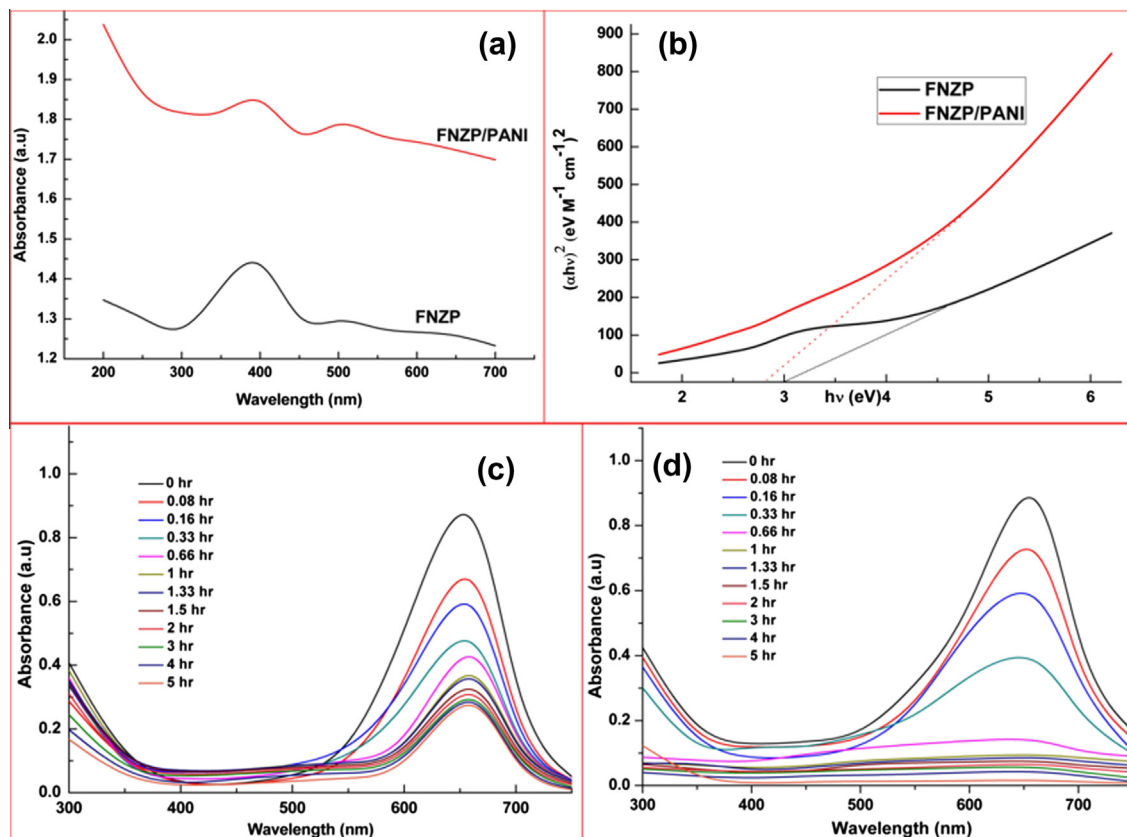


Fig. 5. (a) UV-Visible spectrum of FNZP and FNZP/PANI, (b) Tauc plots for FNZP and FNZP/PANI, (c) absorption spectrum of MB in presence of FNZPs at various times and (d) absorption spectrum of MB in presence of FNZP/PANI at various times.

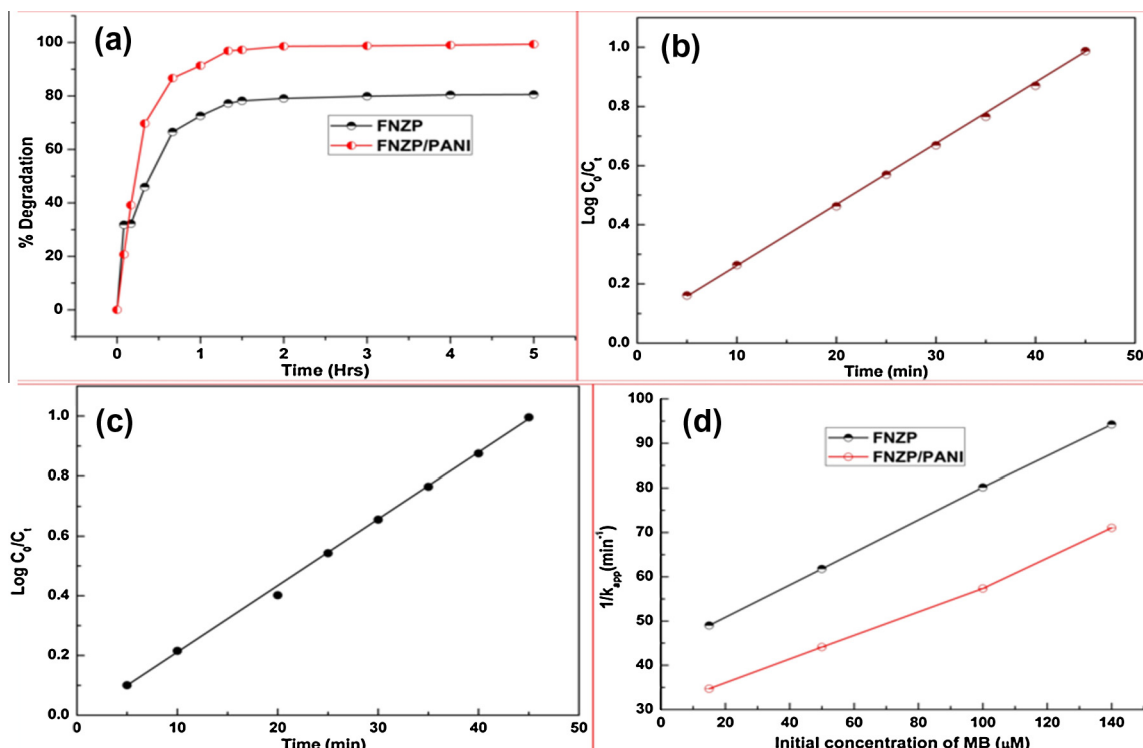


Fig. 6. (a) Extent of decomposition of MB with respect to time in presence of FNZP and FNZP/PANI (b) $\ln C_0/C_t$ vs time for degradation of MB by FNZPs (c) $\ln C_0/C_t$ vs time for degradation of MB by FNZP/PANI and (e) Langmuir–Hinselwood plot.

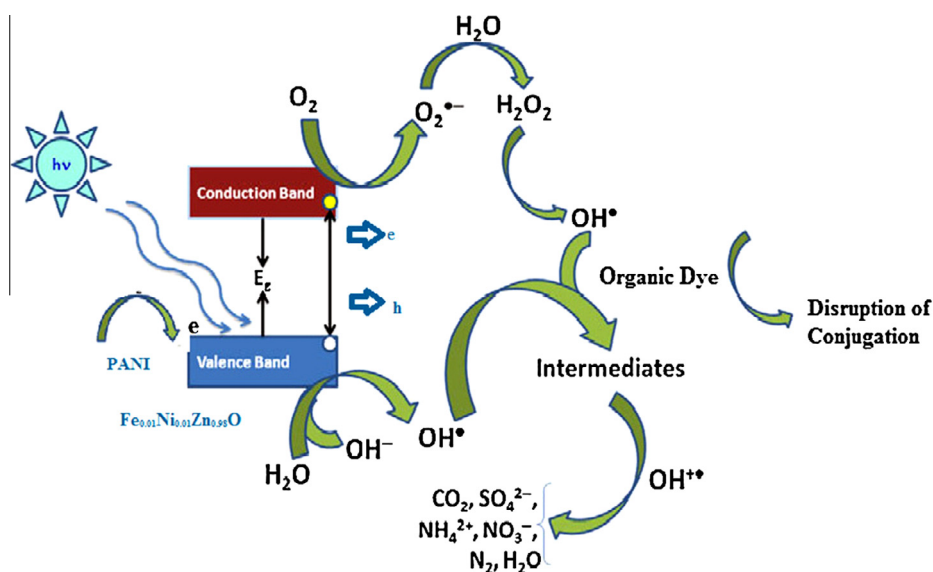


Fig. 7. Proposed mechanism of dye degradation.

bition as it is efficient in low dosages. The effective of FNZP on microorganism can be explained on the basis of the oxygen species (OH^- , H_2O_2 and $\text{O}_2^{\bullet-}$) released on the surface of FNZP, which cause fatal damage to microorganisms. It can be inferred that FNZP/PANI is a better antibacterial agent because low dosage (60 $\mu\text{g}/\text{ml}$) of sample is effective in inhibiting bacterial growth for the complete period of incubation.

Table 2
Comparison of rate constants for various initial concentrations of MB.

Initial concentration of MB (μM)	k_{app} (min^{-1})	
	$\text{Fe}_{0.01}\text{Ni}_{0.01}\text{Zn}_{0.98}\text{O}$	$\text{Fe}_{0.01}\text{Ni}_{0.01}\text{Zn}_{0.98}\text{O}/\text{PANI}$
15	0.020404	0.022361
50	0.016189	0.017106
100	0.012475	0.012928
140	0.010611	0.010985

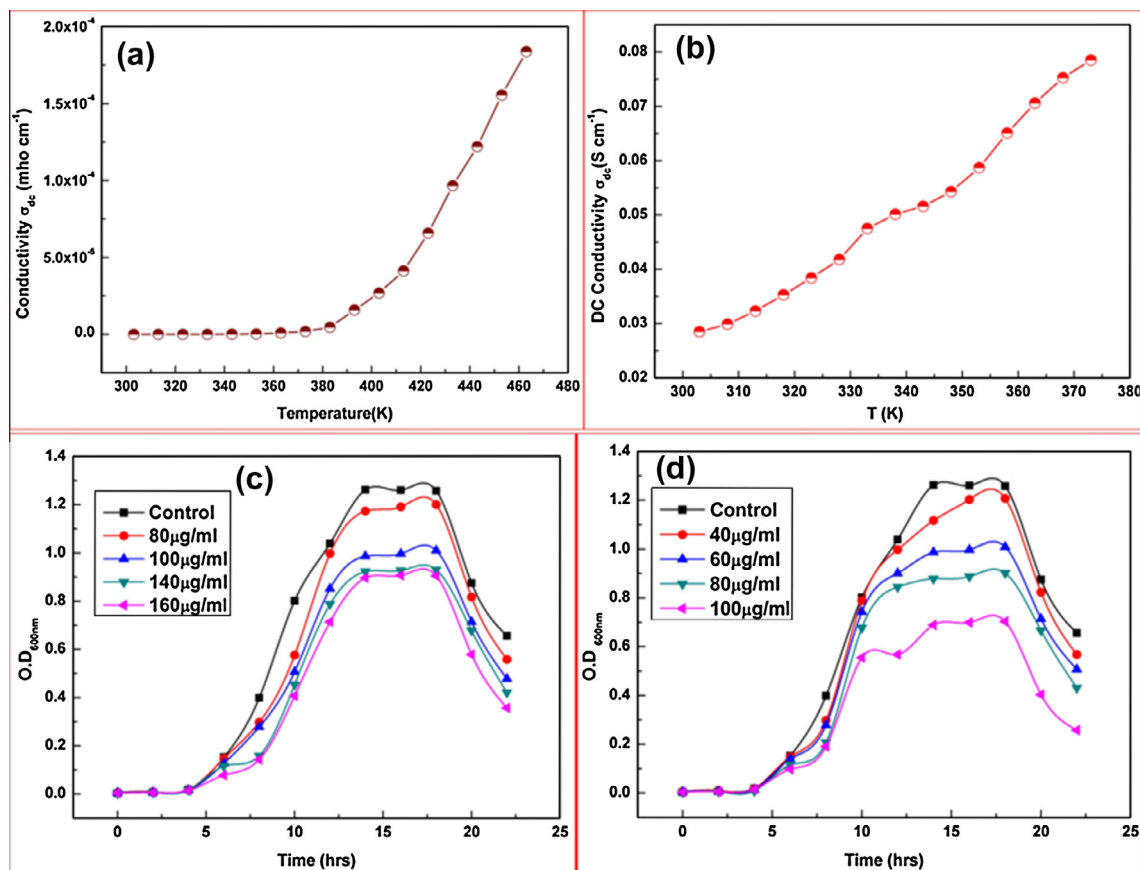


Fig. 8. (a) Variation of DC conductivity of FNZP with temperature, (b) variation of DC conductivity of FNZP/PANI with temperature, (c) O.D curves for bacterial growth in presence of FNZPs and (d) O.D curves for bacterial growth in presence of FNZP/PANI.

4. Conclusions

In summary, novel FNZP/PANI nanocomposite was prepared by free radical in situ polymerisation method. FTIR spectrum confirmed the bonding between FNZP and PANI. The nanocomposites exhibited excellent photocatalytic efficiency against methylene blue under sunlight. A whopping 99.47% dye removal was achieved in 5 h of illumination in case of FNZP/PANI as photocatalyst. The composite exhibits high electrical conductivity at room temperature thus enhancing the property of semiconductor metal oxides. Remarkable antibacterial activity was also obtained because PANI helps in formation of more reactive oxygen species. Thus synthesized nanocomposite promises to be an effective hybrid material for waste water treatment and as an excellent antimicrobial agent.

Acknowledgements

We acknowledge NIPER, Mohali (INDIA) for HRTEM facility and Department of Physics, H.P.U. Shimla and Shoolini University, Solan (India) for necessary facilities.

References

- [1] S. Kango, S. Kalia, A. Celli, J. Njuguna, Y. Habibi, R. Kumar, Surface modification of inorganic nanoparticles for development of organic-inorganic nanocomposites – a review, *Prog. Polym. Sci.*, in press. <<http://dx.doi.org/10.1016/j.progpolymsci.2013.02.003>>.
- [2] A. Moezzi, M.A. McDonagh, B.M. Cortie, *Chem. Eng. J.* 185–186 (2012) 1–22.
- [3] G. MacDiarmid, *Curr. Appl. Phys.* 1 (2001) 269–279.
- [4] S.R. Kargirwar, S.R. Thakare, M.D. Choudhary, S.B. Kondawar, S.R. Dhakate, *Adv. Mat. Lett.* 2 (6) (2011) 397.
- [5] A. Tiwari, R. Kumar, M. Prabhakaran, R.R. Pandey, P. Kumari, A. Chadurvedi, A.K. Mishra, *Polym. Advan. Techno.* 21 (2010) 615.
- [6] Y. Long, Z. Chen, N. Wang, J. Li, M. Wan, *Physica B: Condens. Matter* 344 (2004) 82–87.
- [7] I.S. Lee, J.Y. Lee, J.H. Sung, H.J. Choi, *Synthetic. Met.* 152 (2005) 173–176.
- [8] N.N. Mallikarjun, S.K. Manohar, P.V. Kulkarni, A. Venkataraman, T.M. Aminabhavi, *J. Appl. Polym. Sci.* 97 (2005) 1868–1874.
- [9] J.W. Gilman, *Appl. Clay Sci.* 15 (1999) 31–49.
- [10] D. Porter, E. Metcalfe, M.J.K. Thomas, *Fire Mater.* 24 (2000) 45–52.
- [11] M. Zanetti, S. Lomakin, G. Camino, *Macromol. Mater. Eng.* 279 (2000) 1–9.
- [12] M.D. Bedre, S. Basavaraja, D.S. Balaji, D. Raghunandan, A. Venkataraman, *Inter. J. Polym. Mater.* 59 (2010) 531–543.
- [13] D.Y. Godovski, *Adv. Polym. Sci.* 119 (1995) 79–122.
- [14] P.R. Murray, E.J. Baron, J.H. Jorgensen, M.L. Landry, M.A. Pfaller, *Manual of Clinical Microbiology*, ninth ed., ASM Press, Washington DC, 2009.
- [15] S. Min, F. Wang, F.Y. Han, *J. Mater. Sci.* 42 (2007) 9966–9972.
- [16] W. Feng, E. Sun, A. Fujii, H. Wu, K. Nihara, K. Yoshino, *Bull. Chem. Soc. Jpn.* 73 (2009) 2627–2633.
- [17] N. Faal Hamedani, F. Farzaneh, *J. Sci. Islam. Repub.* 17 (3) (2006) 231–234.
- [18] E.T. Kong, K.G. Neoh, K.L. Tan, *Prog. Polym. Sci.* 23 (1998) 277.
- [19] P.R. Sumari, R. Marimuthu, U.P. Mulik, S.R. Sainkar, D.P. Amelnerkar, *Synthetic. Met.* 106 (1999) 45–52.
- [20] Z. Niu, Z. Yang, Z. Hu, Y. Lu, C.C. Han, *Adv. Funct. Mater.* 13 (2003) 949–954.
- [21] V.B. Patil, S.G. Pawar, S.L. Patil, *J. Mater. Sci. Mater. Electron* 41 (2010) 355–359.
- [22] L.X. Zhang, P. Liu, Z.X. Su, *Polym. Degrad. Stab.* 91 (2006) 2213–2219.
- [23] J. Xu, Y. Ao, D. Fu, C. Yuan, *Appl. Surf. Sci.* 254 (2008) 3033–3038.
- [24] J. Xia, A. Wang, X. Liu, Z. Su, *Appl. Surf. Sci.* 257 (2011) 9724–9732.
- [25] J. Han, P.Q. Mantas, A.M.R. Senos, *J. Eur. Ceram. Soc.* 21 (2001) 1883–1886.
- [26] B.I. Nandapure, S.B. Kondawar, M.Y. Salunke, A.I. Nandapure, *J. Compos. Mater.* 47 (5) (2013) 559–567.